Rapid and Efficient Redox Processes within 2D Covalent Organic Framework Thin Films

Catherine R. DeBlase, Kenneth Hernández-Burgos, Katharine E. Silberstein, Gabriel G. Rodríguez-Calero, Ryan P. Bisbey, Héctor D. Abruña, and William R. Dichtel*

Department of Chemistry and Chemical Biology, Cornell University, Baker Laboratory, Ithaca, New York 14853-1301, United States

ABSTRACT Two-dimensional covalent organic frameworks (2D COFs) are ideally suited for organizing redox-active subunits into periodic, permanently porous polymer networks of interest for pseudocapacitive energy storage. Here we describe a method for synthesizing crystalline, oriented thin films of a redox-active 2D COF on Au working electrodes. The thickness of the COF film was controlled by varying the initial monomer concentration. A large percentage (80−99%) of the anthraquinone groups are electrochemically accessible in films thinner than 200 nm, an order of magnitude improvement over the same COF prepared as a randomly oriented microcrystalline powder. As a result, electrodes functionalized with oriented COF films exhibit a 400% increase in capacitance scaled to electrode area as compared to those functionalized with the randomly oriented COF powder. These results demonstrate the promise of redox-active COFs for electrical energy storage and highlight the importance of controlling morphology for optimal performance.

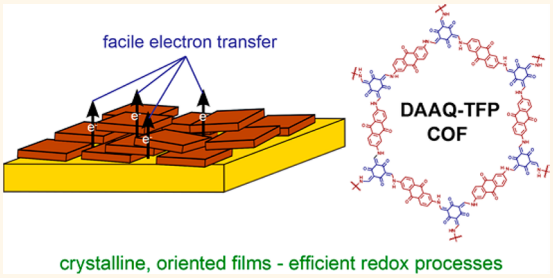

KEYWORDS: covalent organic framework · polymer films · energy storage · supercapacitors · nanoporous materials · electrochemistry · surface science

Electrical energy storage technologies that offer both high power and energy densities have motivated interest in redox-active materials for electrochemical supercapacitors.[1] Supercapacitors store electricity through two distinct processes: the nonfaradaic processes associated with the electrochemical double layer and faradaic processes arising from electrode-bound reversible redox processes, a phenomenon known as pseudocapacitance.[2−6] The electrochemical double layer consists of ions adsorbed to an electrode surface in response to an applied potential and is maximized in high-surface-area electrodes, such as porous carbons.[5,7−15] Redox-active groups may be covalently attached or adsorbed onto these electrodes.[6,16−22] However, these materials are typically not well-defined, which complicates their characterization and rational efforts to improve their performance. Modular and reliable strategies to access high-surface-area electrodes with control over their porosity and surface area as well as the placement and identity of redox-active groups are desirable.

Two-dimensional covalent organic frameworks (2D COFs)[23−26] predictably organize redox-active groups into crystalline, high-surface-area polymer networks with uniform micropores. Electrodes functionalized with 2D COFs might achieve both high theoretical energy density by exhibiting high capacity and high potentials and high power density because their continuous, ordered pores facilitate ion transport. Many early 2D COFs featured boron-containing linkages, which are oxidatively and hydrolytically unstable, limiting their utility as electrode materials, especially at high potentials. However, a new class of COFs linked by β-ketoenamines[27,28] offers superior stability to H_2O, aqueous acid, and high applied potentials. β-Ketoenamine-linked COFs have served as supports for transition metal catalysts[29] and have shown promising proton conductivity.[30] We recently condensed the redox-active monomer 2,6-diaminoanthraquinone (**DAAQ**) with 1,3,5-triformylphluroglucinol (**TFP**) to form the 2D β-ketoenamine-linked **DAAQ-TFP** COF,[31,32] which was the first COF to exhibit reversible

* Address correspondence to wdichtel@cornell.edu.

Received for review January 11, 2015 and accepted February 11, 2015.

Published online February 11, 2015
10.1021/acsnano.5b00184

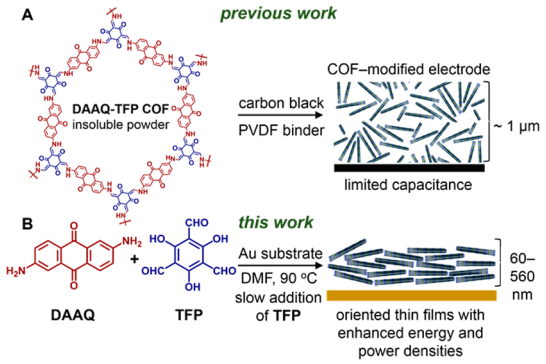

Figure 1. (A) Structure of the hexagonal subunit of the DAAQ-TFP COF, which forms as a 2D-layered microcrystalline powder. This material was previously prepared as a slurry, mixed with carbon black and a PVDF binder, for supercapacitor applications. (B) Solvothermal growth of the DAAQ-TFP COF as an oriented thin film on Au electrodes, a morphology that provides superior electrochemical performance with increased capacitance and enhanced energy and power densities.

redox processes. Electrodes functionalized with a slurry of the **DAAQ-TFP** COF and carbon black were stable for at least 5000 charge–discharge cycles but provided only modest capacitances (~40 F g^{-1}). This modest performance was due, at least in part, to poor electrical contact to the insoluble COF powder samples, so that only a small fraction (~3%) of the redox-active groups were electrochemically accessible (Figure 1A). Here we describe the first oriented thin films[33,34] of β-ketoenamine-linked 2D COFs, which were formed through the slow introduction of the **TFP** monomer into a solution of **DAAQ** in the presence of Au substrates (Figure 1B). **DAAQ-TFP** COF thin films provide near-quantitative addressability of the anthraquinone moieties at thicknesses up to ~200 nm, with areal capacitances of 3.0 mF cm^{-2} (as compared to 0.40 mF cm^{-2} for powder-modified electrodes). These findings demonstrate a means to incorporate 2D COFs into supercapacitors, particularly as lightweight thin-film electrodes on flexible substrates continue to emerge.[12,35–41]

RESULTS AND DISCUSSION

The solvothermal condensation of **DAAQ** and **TFP** in *N*,*N*-dimethylacetamide (DMA) reproducibly generates **DAAQ-TFP** COF as a microcrystalline powder with surface areas >1000 m^2 g^{-1}. However, only nondiffracting β-ketoenamine-linked films were formed when Au substrates were included in reactions performed under similar conditions. We hypothesized that the polymerization occurred too rapidly to yield crystalline films and found that the slow addition (over 1 h) of a DMF solution of **TFP** into a DMF solution of **DAAQ** at 90 °C generated crystalline, oriented films, as determined by grazing incidence X-ray diffraction (GID). The films were characterized by infrared spectroscopy (FTIR), which indicated the disappearance of the N–H stretch region with the emergence of a new C–N stretch at 1250 cm^{-1} and a C=C stretch at 1560 cm^{-1}. These absorbances are characteristic of β-ketoenamine C–N and C=C bonds, respectively, and match those found in the FTIR spectra of a model compound and microcrystalline powder of **DAAQ-TFP** COF (Supporting Information Figure S1). Furthermore, the C=O stretch found in the **TFP** monomer at 1658 cm^{-1} shifts to 1615 cm^{-1}, consistent with the C=O of the β-ketoenamine linkage. X-ray photoelectron spectroscopy (XPS) of the films also suggested the formation of the expected enamine linkages in the COF films (Figure S2). **DAAQ-TFP** COF powders exhibit a N_{1s} binding energy of 399.2 eV that corresponds to the β-ketoenamine nitrogen, and the **DAAQ** monomer N_{1s} binding energy is 398.4 eV (ΔE = 0.8 eV). Both of these N_{1s} peaks shift to lower energy for the **DAAQ** monomer or COF film on Au substrates (398.5 and 397.7 eV for the **DAAQ** monomer and **DAAQ-TFP** COF, respectively) but retain the characteristic energy difference (0.8 eV) between aniline and enamine N_{1s} signals. These spectroscopic signatures, combined with X-ray diffraction of the films (see below), confirm the formation of the expected **DAAQ-TFP** COF thin films.

Under the above thin-film growth conditions, varying the initial monomer concentration provided control of the resulting film thickness. Films grown at an initial **DAAQ** concentration ($[\mathbf{DAAQ}]_0$) of 22 mM were 484 ± 80 nm thick (average of five substrates, as determined by AFM, Figure S3). GIXD of these films exhibit a prominent (100) peak corresponding to a $Q_{\parallel}$ of 0.23 $Å^{-1}$ (Figure 2, top). The vertical orientation of the stacking direction with respect to the substrate is indicated by the presence of the (001) peak centered at $Q_{\perp}$ = 1.8 $Å^{-1}$ and $Q_{\parallel}$ = 0 (Figure 2, inset). Films grown at $[\mathbf{DAAQ}]_0$ = 11 mM were 310 ± 70 nm thick and provide similar, albeit weaker, diffraction patterns. Films grown at 2.2 mM were still thinner (106 ± 27 nm) and did not exhibit a (100) diffraction peak associated with periodicity in the plane of covalent bonding. Nevertheless, the (001) peaks at $Q_{\perp}$ = 1.8 $Å^{-1}$ and $Q_{\parallel}$ = 0 are observed, indicating a vertically oriented, layered structure. These films exhibit FTIR and XPS spectra identical to that of the thicker samples, as well as consistent electrochemical performance (see below), suggesting that their chemical composition is identical. It is unclear whether thin films are more disordered in-plane or if all films contain a mixture of amorphous and crystalline domains, such that a higher threshold thickness is needed before diffraction at small $Q_{\perp}$ is observed.

Cyclic voltammetry (CV) experiments indicate that a large percentage of the anthraquinone moieties in the **DAAQ-TFP** films are electroactive, a major improvement compared to the approximately 3% accessed in electrodes functionalized with a slurry of the powder. The voltammogram of a 180 nm thick film in 1 M H_2SO_4 supporting electrolyte exhibits a current onset of 0.1 V

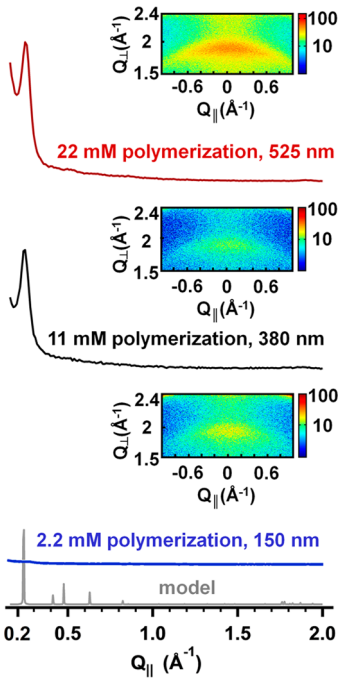

Figure 2. One-dimensional projections at low values of $Q_\perp$ of the GIDs obtained for DAAQ-TFP COF films show diffraction peaks when grown at higher monomer concentrations (22 mM, red, or 11 mM, black). Films grown under more dilute conditions (2.2 mM, blue) do not show in-plane diffraction peaks. Insets: Diffraction associated with the out-of-plane (001) stacking peak for the 22, 11, and 2.2 mM polymerizations, respectively, indicates that each film forms an oriented, layered structure.

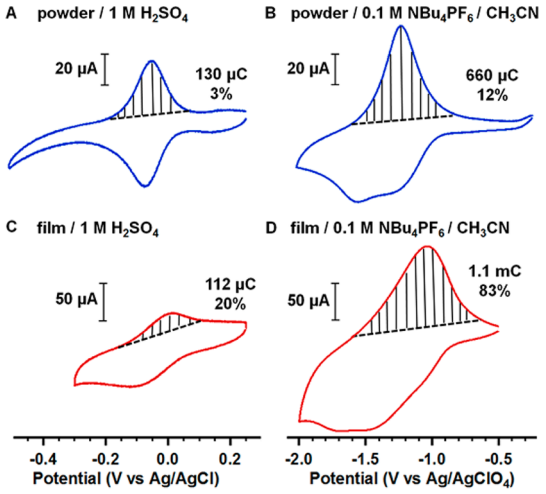

Figure 3. Cyclic voltammograms (50 mV s^{-1}) of (A) DAAQ-TFP COF slurry-modified electrode in 1 M aqueous H_2SO_4, (B) DAAQ-TFP COF slurry-modified electrode in 0.1 M NBu_4PF_6 in CH_3CN. (C,D) Cyclic voltammograms for a DAAQ-TFP thin film (180 nm) in 1.0 M H_2SO_4 and 0.1 M NBu_4PF_6 in CH_3CN, respectively. The integrated charge of the oxidative wave and percentage of quinones accessed are listed for each voltammogram.

vs Ag/AgCl, which is associated with anthraquinone reduction. Integration of the corresponding oxidative wave provides a charge (112 μC) that corresponds to approximately 20% of the anthraquinones being redox-active, based on the geometric area of the electrode and film thickness (see Supporting Information for calculation). This improvement is also apparent by comparing the currents generated by the film and slurry-modified electrodes, given that the slurry-modified electrode contains approximately 10 times the mass of the **DAAQ-TFP COF**. Despite this improvement, the **DAAQ-TFP** film CV indicates high resistance, for which careful analysis of the electrochemical data presented in Figure 3 provides additional insight. The voltammetric profile in Figure 3A (slurry-modified electrode) exhibits faster charge transfer kinetics than that in Figure 3C (thin-film-modified electrode), as indicated by its smaller ΔE_p value.[42] The thin-film voltammogram exhibits both slower charge transfer and higher resistance. Yet, the percentage of the quinones accessed in the thin films is much higher. We speculate that the differences in the voltammetric profiles are due, at least in part, to the different nature of the modified electrodes and the redox reactions involved. The slurry-modified electrodes consist of a 60:35:5 weight ratio of carbon black, COF, and binder (PVDF), respectively, whereas the COF thin-film electrodes are solid films that lack the carbon or binder. In the 1 M H_2SO_4 supporting electrolyte, the redox reaction involves the transfer of two electrons and two protons per quinone moiety. For the slurry-modified electrodes, the exposed redox-active quinone sites are accessible to protons, providing a rapid voltammetric response, but only this small fraction of the quinones are accessed. For the thin-film electrode, proton transfer is more difficult, providing slower charge transfer, but a much larger fraction of the quinones is accessed. We attribute the improved accessibility to the layered organization of quinone groups in the solid film, enabling conductivity through electron self-exchange processes. Panels B and D of Figure 3 compare the voltammetric responses of the two electrode types in an aprotic supporting electrolyte (0.1 M NBu_4PF_6/CH_3CN). Here the redox reactions do not involve protonation, and the voltammetric profiles look qualitatively similar. However, the ability of the solid COF film to undergo effective self-exchange is retained, and thus a much higher percent (83%) of the quinone groups are accessed. This model, while speculative, is consistent with all of our electrochemical data of this system.

In addition to the significantly enhanced electrochemical performance, CH_3CN also provides a wider potential window that enhances the double-layer capacitance of the system. The improvement in acetonitrile is relatively modest (from 3 to 12%) for the powder-functionalized electrodes but is much more dramatic for the oriented thin films (from 20 to 40−99%, Figure 3). A survey of 11 films of varying thickness indicated that nearly all of the anthraquinones are redox-active within films ≤184 nm thick (Table 1). This percentage decreases in thicker films (83−41% for

TABLE 1. Film Thickness, Integrated Charge of the Oxidative Wave, and Percent of Anthraquinones Accessed in the Films[a]

film thickness (nm)	charge (μC)	quinones accessed (%)
77	513	91
101	722	98
115	672	80
147	1049	99
150	930	85
184	1135	85
228	949	57
232	1013	60
280	1693	83
346	1547	62
348	1031	41

[a] The integrated charges were determined from cyclic voltammograms obtained at 50 mV s^{-1} in 0.1 M NBu_4PF_6/CH_3CN supporting electrolyte. The line identifies the upper limit to film thickness allowing quantitative quinone access.

228–348 nm films). However, it should be noted that the thickest films contain similar amounts of COF as the slurry-modified electrodes with a 4- to 6-fold increase in accessible quinones. We attribute this to the oriented crystallite morphology of the **DAAQ-TFP** thin films, making redox conduction between layers of anthraquinones and different crystallites more facile than in a randomly oriented sample. Indeed, when a CV of a randomly oriented COF-modified electrode is obtained in the presence of anthraquinone dissolved in the supporting electrolyte, the quinone addressability increases from 12 to 27% (Figure S12), further demonstrating the role of anthraquinone–anthraquinone charge transfer ("self-exchange") present in oriented thin films. We also identified the practical upper limit of film thickness as 300–400 nm. A 348 nm crystalline, oriented film shows a quasi-reversible quinone peak at $E^{\circ\prime}$ of −1.4 V *vs* $Ag/AgClO_4$ when scanned at 1 mV s^{-1}, which represents 59% of available quinones. However, these redox waves are not observed at the 50 mV s^{-1} scan rates employed in Figure 3 and Table 1, indicating that the resistance dominates the electrochemical response of thicker films at this scan rate (Figure 4). For efficient redox conduction to occur, the cations in the supporting electrolyte must be able to move throughout the COF film to compensate the negative charge injected into the film. Below approximately 200 nm, the film thickness appears optimal for this process, as quantitative quinone addressability is obtained. In thicker films, electrolyte diffusion to the electrode surface occurs more slowly, such that the current response becomes dominated by the sample's resistance. This trend was further confirmed through electrochemical impedance spectroscopy, as the impedance response at the high-frequency limit (represented by R_{sol} in the model; see Supporting Information) increased from 500 to 1100 Ω (see Table 2) in 60 and 170 nm films, respectively. Finally, although films thinner than 200 nm generally show increased quinone addressability, some variability is observed, even among films of similar thickness. These differences might arise from variations in the film morphology, grain boundaries, or contamination by residual monomers and/or oligomers. Improved characterization and control of COF film growth are needed to probe these questions further.

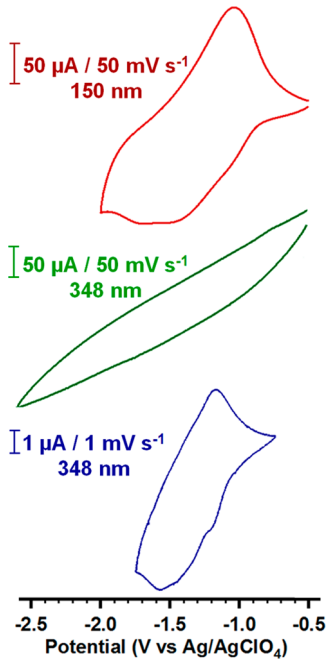

Figure 4. Cyclic voltammogram of a 180 nm thick DAAQ-TFP thin film (red, 0.1 M $TBAPF_6$/MeCN supporting electrolyte, 50 mV s^{-1}) compared to a 348 nm DAAQ-TFP COF film recorded under identical conditions (green). The blue CV is the same 348 nm film scanned at a slower scan rate of (1 mV s^{-1}), confirming the presence of the anthraquinones in the thicker samples, whose response is dominated by resistance at faster scan rates.

TABLE 2. Relationship between Solution Resistance and Film Thickness[a]

height (nm)	R_{sol} (Ω)
173	1100
156	673
150	690
60	515

[a] R_{sol} was determined from fitting impedance spectra to the model displayed in the Supporting Information and is the intersection of the impedance data with Z' at a high frequency of alternating potential applied.

The capacitance of each film was determined using galvanostatic charge–discharge cycles (GCDC), in which the potential response as a function of time is measured at constant current. The charge polarity is reversed when the potential reaches a predetermined limit, such that one measurement cycle characterizes both the charging and discharging processes of the electrode under test. GCDC of the **DAAQ-TFP**-functionalized electrodes at current densities of 150 μA cm^{-2} (an approximate *C* rate of 80) exhibited voltage–time profiles with voltage plateaus at the

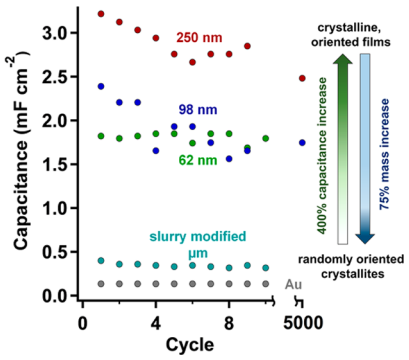

Figure 5. Thin-film capacitances derived from GCDC experiments. A current density of 150 μA cm^{-2} was used. A DAAQ-TFP COF slurry-modified electrode (teal) and blank Au electrode (gray) show low capacitance values. Oriented thin films each show improved capacitance as a function of thickness: 250 nm (red), 98 nm (blue), and 62 nm (green).

potential of anthraquinone reduction (see Supporting Information). Films of various thicknesses exhibited stable capacitances ranging from 1.2 to 3.0 mF cm^{-2} over 10 cycles. Two of these films were selected for extended testing and showed ~7% capacitance loss from their stabilized values after 5000 cycles, indicating the high stability of the β-ketoenamine framework (Figure 5). All films show a higher capacitance compared to a randomly oriented slurry-modified electrode or blank gold substrate, which stabilized around 0.40 or 0.13 mF cm^{-2}, respectively.

CONCLUSIONS

The first oriented thin films of β-ketoenamine COFs were formed through the slow introduction of the **DAAQ** monomer into a solution of **TFP** in the presence of Au substrates. The film thickness was controlled by varying the initial concentrations of the monomers. In contrast to working electrodes functionalized with samples of the randomly oriented COF slurry, the **DAAQ-TFP** COF thin films show improved accessibility of their redox-active anthraquinone moieties. GCDC experiments indicate that, by using oriented crystalline thin films, we have drastically improved the charge storage capabilities of **DAAQ-TFP** COF from 0.4 to 3 mF cm^{-2}. These findings demonstrate the importance of controlling the morphology of 2D COFs in order to take full advantage of their desirable properties, including their high specific surface area, oriented micro- or mesopores, and redox behavior. These findings will inform future efforts to prepare COFs relevant for optoelectronic and other energy storage applications.

METHODS

Material Characterization. COF films were grown from solution on Au substrates, which were prepared by sputtering a Ti or Cr adhesion layer (~15 nm) followed by Au (80 nm) onto a Si wafer. FTIR spectra of the films were obtained on a Bruker Vertex 80v instrument with a germanium ATR attachment. XPS was performed on a Surface Science Instruments X-Probe (SSX-100), and AFMs were done on an Asylum MFP3D-Bio AFM.

Electrochemical Characterization. Electrochemistry experiments were performed on a Princeton Applied Research VersaSTAT 3 potentiostat using a standard three-electrode setup, with the COF film on Au as the working electrode, Pt coil as the counter electrode, and a $Ag/AgClO_4$ reference electrode standardized with ferrocene. Analysis was performed in a nitrogen-filled glovebox using a custom-designed glass surface cell having a controlled exposed area of 0.64 cm^2 with 0.1 M $TBAPF_6$ in CH_3CN as the electrolyte. Voltammograms taken in aqueous H_2SO_4 supporting electrolyte were performed on the bench after sparging with argon to remove O_2. Impedance spectra were taken on a Gamry Instruments potentiostat on the bench under an Ar atmosphere.

Conflict of Interest: The authors declare no competing financial interest.

Acknowledgment. This research was supported by the NSF in the form of an NSF GRFP (DGE-1144153) award to C.R.D. W.R.D. acknowledges the Alfred P. Sloan Foundation for a Sloan Research Fellowship and the Camille and Henry Dreyfus Foundation for a Camille Dreyfus Teacher-Scholar Award. R.P.B. acknowledges support from the NSF IGERT program (DGE-0903653). This work was supported in part (K.H.B., K.E.S., G.R.C., H.D.A.) by the DOE through Grant DE-FG02-87ER45298, by the Energy Materials Center at Cornell (emc^2), an Energy Frontier Research Center funded by the DOE Office of Basic Energy Sciences (DE-SC000001086), and an Innovation Economy Matching Grant from the New York State, Empire State Development Division of Science, Technology and Innovation (NYSTAR), under Contract No. C090148. K.E.S. was supported by a fellowship from the Cornell High Energy Synchrotron Source (CHESS) under NSF Award PHY-936384. CHESS is supported by the NSF and NIH/NIGMS *via* NSF award DMR-1332208. This research made use of the Cornell Center for Materials Research Facilities supported by the NSF (DMR-1120296). This work made use of the Nanobiotechnology Center shared research facilities at Cornell.

Supporting Information Available: Experimental details, additional electrochemical data, and analysis. This material is available free of charge *via* the Internet at http://pubs.acs.org.

REFERENCES AND NOTES

1. Goodenough, J. B.; Buchanan, M.; Abruña, H. D. *Basic Research Needs for Electrical Energy Storage*; Office of Basic Sciences, U.S. Department of Energy, **2007**.
2. Abruña, H. D.; Kiya, Y.; Henderson, J. C. Batteries and Electrochemical Capacitors. *Phys. Today* **2008**, *61*, 43–47.
3. Wang, G.; Zhang, L.; Zhang, J. A Review of Electrode Materials for Electrochemical Supercapacitors. *Chem. Soc. Rev.* **2012**, *41*, 797–828.
4. Winter, M.; Brodd, R. J. What Are Batteries, Fuel Cells, and Supercapacitors? *Chem. Rev.* **2004**, *104*, 4245–4270.
5. Merlet, C.; Rotenberg, B.; Madden, P. A.; Taberna, P.-L.; Simon, P.; Gogotsi, Y.; Salanne, M. On the Molecular Origin of Supercapacitance in Nanoporous Carbon Electrodes. *Nat. Mater.* **2012**, *11*, 306–310.
6. Rauda, I. E.; Augustyn, V.; Dunn, B.; Tolbert, S. H. Enhancing Pseudocapacitive Charge Storage in Polymer Templated Mesoporous Materials. *Acc. Chem. Res.* **2013**, *46*, 1113–1124.
7. Chmiola, J.; Yushin, G.; Gogotsi, Y.; Portet, C.; Simon, P.; Taberna, P. L. Anomalous Increase in Carbon Capacitance at Pore Sizes Less than 1 Nanometer. *Science* **2006**, *313*, 1760–1763.
8. Simon, P.; Gogotsi, Y. Capacitive Energy Storage in Nanostructured Carbon–Electrolyte Systems. *Acc. Chem. Res.* **2013**, *46*, 1094–1103.

9. Zhu, Y.; Murali, S.; Stoller, M. D.; Ganesh, K. J.; Cai, W.; Ferreira, P. J.; Pirkle, A.; Wallace, R. M.; Cychosz, K. A.; Thommes, M.; et al. Carbon-Based Supercapacitors Produced by Activation of Graphene. *Science* **2011**, *332*, 1537–1541.
10. Volder, M. F. L. D.; Tawfick, S. H.; Baughman, R. H.; Hart, A. J. Carbon Nanotubes: Present and Future Commercial Applications. *Science* **2013**, *339*, 535–539.
11. Choi, N.-S.; Chen, Z.; Freunberger, S. A.; Ji, X.; Sun, Y.-K.; Amine, K.; Yushin, G.; Nazar, L. F.; Cho, J.; Bruce, P. G. Challenges Facing Lithium Batteries and Electrical Double-Layer Capacitors. *Angew. Chem., Int. Ed.* **2012**, *51*, 9994–10024.
12. Chmiola, J.; Largeot, C.; Taberna, P.-L.; Simon, P.; Gogotsi, Y. Monolithic Carbide-Derived Carbon Films for Micro-Supercapacitors. *Science* **2010**, *328*, 480–483.
13. Han, J.; Zhang, L. L.; Lee, S.; Oh, J.; Lee, K.-S.; Potts, J. R.; Ji, J.; Zhao, X.; Ruoff, R. S.; Park, S. Generation of B-Doped Graphene Nanoplatelets Using a Solution Process and Their Supercapacitor Applications. *ACS Nano* **2013**, *7*, 19–26.
14. Gogotsi, Y.; Nikitin, A.; Ye, H.; Zhou, W.; Fischer, J. E.; Yi, B.; Foley, H. C.; Barsoum, M. W. Nanoporous Carbide-Derived Carbon with Tunable Pore Size. *Nat. Mater.* **2003**, *2*, 591–594.
15. Xu, Y.; Sheng, K.; Li, C.; Shi, G. Self-Assembled Graphene Hydrogel *via* a One-Step Hydrothermal Process. *ACS Nano* **2010**, *4*, 4324–4330.
16. Wang, Y.; Bai, Y.; Li, X.; Feng, Y.; Zhang, H. A General Strategy towards Encapsulation of Nanoparticles in Sandwiched Graphene Sheets and the Synergic Effect on Energy Storage. *Chem.—Eur. J.* **2013**, *19*, 3340–3347.
17. Benson, J.; Boukhalfa, S.; Magasinski, A.; Kvit, A.; Yushin, G. Chemical Vapor Deposition of Aluminum Nanowires on Metal Substrates for Electrical Energy Storage Applications. *ACS Nano* **2012**, *6*, 118–125.
18. Dai, L. Functionalization of Graphene for Efficient Energy Conversion and Storage. *Acc. Chem. Res.* **2013**, *46*, 31–42.
19. Huang, H.; Nazar, L. F. Grafted Metal Oxide/Polymer/Carbon Nanostructures Exhibiting Fast Transport Properties. *Angew. Chem., Int. Ed.* **2001**, *40*, 3880–3884.
20. Kurra, N.; Alhebshi, N. A.; Alshareef, H. N. Microfabricated Pseudocapacitors Using $Ni(OH)_2$ Electrodes Exhibit Remarkable Volumetric Capacitance and Energy Density. *Adv. Energy Mater.* **2015**, 1401303.
21. Du, F.; Yu, D.; Dai, L.; Ganguli, S.; Varshney, V.; Roy, A. K. Preparation of Tunable 3D Pillared Carbon Nanotube–Graphene Networks for High-Performance Capacitance. *Chem. Mater.* **2011**, *23*, 4810–4816.
22. Mai, L.-Q.; Minhas-Khan, A.; Tian, X.; Hercule, K. M.; Zhao, Y.-L.; Lin, X.; Xu, X. Synergistic Interaction between Redox-Active Electrolyte and Binder-Free Functionalized Carbon for Ultrahigh Supercapacitor Performance. *Nat. Commun.* **2013**, *4*, 1–7.
23. Feng, X.; Ding, X.; Jiang, D. Covalent Organic Frameworks. *Chem. Soc. Rev.* **2012**, *41*, 6010–6022.
24. Ding, S.-Y.; Wang, W. Covalent Organic Frameworks (COFs): From Design to Applications. *Chem. Soc. Rev.* **2013**, *42*, 548–568.
25. Colson, J. W.; Dichtel, W. R. Rationally Synthesized Two-Dimensional Polymers. *Nat. Chem.* **2013**, *5*, 453–465.
26. Côté, A. P.; Benin, A. I.; Ockwig, N. W.; O'Keeffe, M.; Matzger, A. J.; Yaghi, O. M. Porous, Crystalline, Covalent Organic Frameworks. *Science* **2005**, *310*, 1166–1170.
27. Kandambeth, S.; Mallick, A.; Lukose, B.; Mane, M. V.; Heine, T.; Banerjee, R. Construction of Crystalline 2D Covalent Organic Frameworks with Remarkable Chemical (Acid/Base) Stability *via* a Combined Reversible and Irreversible Route. *J. Am. Chem. Soc.* **2012**, *134*, 19524–19527.
28. Biswal, B. P.; Chandra, S.; Kandambeth, S.; Lukose, B.; Heine, T.; Banerjee, R. Mechanochemical Synthesis of Chemically Stable Isoreticular Covalent Organic Frameworks. *J. Am. Chem. Soc.* **2013**, *135*, 5328–5331.
29. Pachfule, P.; Panda, M. K.; Kandambeth, S.; Shivaprasad, S. M.; Díaz, D. D.; Banerjee, R. Multifunctional and Robust Covalent Organic Framework–Nanoparticle Hybrids. *J. Mater. Chem. A* **2014**, *2*, 7944–7952.
30. Chandra, S.; Kundu, T.; Kandambeth, S.; BabaRao, R.; Marathe, Y.; Kunjir, S. M.; Banerjee, R. Phosphoric Acid Loaded Azo (–N=N–) Based Covalent Organic Framework for Proton Conduction. *J. Am. Chem. Soc.* **2014**, *136*, 6570–6573.
31. DeBlase, C. R.; Silberstein, K. E.; Truong, T.-T.; Abruña, H. D.; Dichtel, W. R. B-Ketoenamine-Linked Covalent Organic Frameworks Capable of Pseudocapacitive Energy Storage. *J. Am. Chem. Soc.* **2013**, *135*, 16821–16824.
32. Colson, J. W.; Woll, A. R.; Mukherjee, A.; Levendorf, M. P.; Spitler, E. L.; Shields, V. B.; Spencer, M. G.; Park, J.; Dichtel, W. R. Oriented 2D Covalent Organic Framework Thin Films on Single-Layer Graphene. *Science* **2011**, *332*, 228–231.
33. Spitler, E. L.; Colson, J. W.; Uribe-Romo, F. J.; Woll, A. R.; Giovino, M. R.; Saldivar, A.; Dichtel, W. R. Lattice Expansion of Highly Oriented 2D Phthalocyanine Covalent Organic Framework Films. *Angew. Chem., Int. Ed.* **2012**, *51*, 2623–2627.
34. Colson, J. W.; Mann, J. A.; DeBlase, C. R.; Dichtel, W. R. Patterned Growth of Oriented 2D Covalent Organic Framework Thin Films on Single-Layer Graphene. *J. Polym. Sci., Part A: Polym. Chem.* **2014**, *53*, 378–384.
35. Pushparaj, V. L.; Shaijumon, M. M.; Kumar, A.; Murugesan, S.; Ci, L.; Vajtai, R.; Linhardt, R. J.; Nalamasu, O.; Ajayan, P. M. Flexible Energy Storage Devices Based on Nanocomposite Paper. *Proc. Natl. Acad. Sci. U.S.A.* **2007**, *104*, 13574–13577.
36. Hong, S. Y.; Yoon, J.; Jin, S. W.; Lim, Y.; Lee, S.-J.; Zi, G.; Ha, J. S. High-Density, Stretchable, All-Solid-State Microsupercapacitor Arrays. *ACS Nano* **2014**, *8*, 8844–8855.
37. Xu, P.; Kang, J.; Choi, J.-B.; Suhr, J.; Yu, J.; Li, F.; Byun, J.-H.; Kim, B.-S.; Chou, T.-W. Laminated Ultrathin Chemical Vapor Deposition Graphene Films Based Stretchable and Transparent High-Rate Supercapacitor. *ACS Nano* **2014**, *8*, 9437–9445.
38. El-Kady, M. F.; Strong, V.; Dubin, S.; Kaner, R. B. Laser Scribing of High-Performance and Flexible Graphene-Based Electrochemical Capacitors. *Science* **2012**, *335*, 1326–1330.
39. Kaempgen, M.; Chan, C. K.; Ma, J.; Cui, Y.; Gruner, G. Printable Thin Film Supercapacitors Using Single-Walled Carbon Nanotubes. *Nano Lett.* **2009**, *9*, 1872–1876.
40. Choi, K. M.; Jeong, H. M.; Park, J. H.; Zhang, Y.-B.; Kang, J. K.; Yaghi, O. M. Supercapacitors of Nanocrystalline Metal–Organic Frameworks. *ACS Nano* **2014**, *8*, 7451–7457.
41. Gao, S.; Sun, Y.; Lei, F.; Liang, L.; Liu, J.; Bi, W.; Pan, B.; Xie, Y. Ultrahigh Energy Density Realized by a Single-Layer B-$Co(OH)_2$ All-Solid-State Asymmetric Supercapacitor. *Angew. Chem., Int. Ed.* **2014**, *53*, 12789–12793.
42. Frackowiak, E.; Béguin, F. Carbon Materials for the Electrochemical Storage of Energy in Capacitors. *Carbon* **2001**, *39*, 937–950.